Search for Dark Photons with Superconducting Radio Frequency Cavities

A. Romanenko,[1,*] R. Harnik,[1,†] A. Grassellino,[1,‡] R. Pilipenko,[1] Y. Pischalnikov,[1] Z. Liu,[2,§] O. S. Melnychuk,[1] B. Giaccone,[1] O. Pronitchev,[1] T. Khabiboulline,[1] D. Frolov,[1] S. Posen,[1] S. Belomestnykh,[1] A. Berlin,[1] and A. Hook[3]

[1]*Fermi National Accelerator Laboratory, Batavia, Illinois 60510, USA*

[2]*School of Physics and Astronomy, University of Minnesota, Minneapolis, Minnesota 55455, USA*

[3]*Maryland Center for Fundamental Physics, University of Maryland, College Park, Maryland 20742, USA*

(Received 28 January 2023; accepted 23 May 2023; published 26 June 2023)

We conduct the first "light-shining-through-wall" (LSW) search for dark photons using two state-of-the-art high-quality-factor superconducting radio frequency (SRF) cavities —Dark SRF—and report the results of its pathfinder run. Our new experimental setup enables improvements in sensitivity over previous searches and covers new dark photon parameter space. We design delicate calibration and measurement protocols to utilize the high-Q setup at Dark SRF. Using cavities operating at 1.3 GHz, we establish a new exclusion limit for kinetic mixing as small as $\epsilon = 1.6 \times 10^{-9}$ and provide the world's best constraints on dark photons in the 2.1×10^{-7}–5.7×10^{-6} eV mass range. Our result is the first proof of concept for the enabling role of SRF cavities in LSW setups, with ample opportunities for further improvements. In addition, our data set a competitive lab-based limit on the standard model photon mass by searching for longitudinal photon polarization.

DOI: 10.1103/PhysRevLett.130.261801

Introduction.—One of the conceptually simplest proposed extensions to the standard model (SM) of particle physics is the existence of a hidden sector consisting of particles feebly coupled to ordinary matter. In particular, the hypothesized "dark photon" [1] interacts with ordinary matter via a small kinetic mixing with the SM photon. A range of possible photon-dark photon couplings ϵ and dark photon masses $m_{\gamma'}$ has been previously excluded based on the combination of laboratory experiments and astrophysical observations [2,3].

Several lab-based dark photon searches have been performed using the "light-shining-through-wall" (LSW) scheme [4–6]. These experiments involve a source of SM photons at a particular frequency (e.g., laser light), a wall impenetrable to this light, and a detector looking for photons of the same frequency that emerge past the wall. The emission of some of the photons as dark photons before the wall and their detection after the wall makes such a search possible if dark photons exist with a hypothesized mass and coupling. Resonant cavities can be used both to increase the number of photons on the emitting side and to enhance the detection probability on the receiver side. This scheme has been implemented successfully in the optical [7] and microwave frequency regimes [8,9].

The use of superconducting microwave cavities in LSW experiments was proposed in Ref. [10], and an optimal relative cavity orientation to emit and detect the longitudinal dark photon polarization was later identified in Ref. [11]. Compared to optical light, microwaves enable simpler cavity engineering, readout, and ultrahigh quality factors. The most recent LSW microwave experiments utilized two normal-conducting cavities with loaded quality factors of $Q \sim 10^3$–10^4 [8,9]. Superconducting radio frequency (SRF) cavities routinely utilized in modern particle accelerators [12–14] have intrinsic quality factors of $Q > 10^{10}$, providing a unique opportunity for multiple orders of magnitude enhancement both in the number of stored photons in the "emitter" cavity and in the detection sensitivity of the "receiver" cavity. In this Letter, we present the first results of Dark SRF, a LSW experiment utilizing such ultrahigh quality factor SRF cavities with the optimal arrangement for longitudinal dark photon detection.

Dark photon and signal power.—The dark photon A'_μ is a massive vector boson of mass $m_{\gamma'}$ which interacts with the SM via

$$\mathcal{L} = \mathcal{L}_{\mathrm{SM}} - \frac{1}{4} F'_{\mu\nu} F'^{\mu\nu} + \frac{\epsilon}{2} F'_{\mu\nu} F^{\mu\nu} + \frac{1}{2} m_{\gamma'}^2 A'_\mu A'^{\mu}, \quad (1)$$

where F and F' are the field strengths of the photon and dark photon, and ϵ is a small kinetic mixing parameter which couples the SM and dark electromagnetic fields [1–3]. As a result, a coherently oscillating SM electromagnetic field acts as a source of dark photons at the same frequency. In addition, a coherent dark photon

field can resonantly excite a rf cavity with the appropriate frequency.

Given an emitter cavity with intrinsic quality factor Q_{em} and stored energy U_{em}, the radiated dark photon field will then deposit power in a nearby receiver cavity with intrinsic quality factor Q_{rec},

$$P_{\mathrm{rec}} = \epsilon^4 \left(\frac{m_{\gamma'}}{\omega}\right)^4 |G|^2 \omega Q_{\mathrm{rec}} U_{\mathrm{em}}, \tag{2}$$

where G is a form factor specified in the Appendix, which heuristically consists of the wave function overlap of the dark photon field with the spatial mode shape in the receiver cavity. As pointed out in Ref. [11], when the cavities are oriented to produce and detect the longitudinal polarization of the dark photon field, the right-hand side of Eq. (2) is suppressed by the fourth power of mass over frequency rather than the eighth power, as was the case in the dark photon search in the CROWS experiment [8,9], which was optimized for the transverse mode [15]. Assuming that the dominant noise in the receiver is thermal in nature, the signal-to-noise ratio (SNR) is given by the radiometer formula [16]:

$$\mathrm{SNR} = \frac{P_{\mathrm{rec}}}{P_{\mathrm{th}}} \sqrt{\delta\nu t_{\mathrm{int}}} = \frac{P_{\mathrm{rec}}}{k_B T_{\mathrm{eff}}} \sqrt{\frac{t_{\mathrm{int}}}{\delta\nu}}, \tag{3}$$

where $\delta\nu$ is the bandwidth of the analysis, t_{int} is the integration time, T_{eff} is the effective noise temperature, and $P_{\mathrm{th}} = k_B T_{\mathrm{eff}} \delta\nu$ is the noise power. The factor of $\sqrt{\delta\nu t_{\mathrm{int}}}$ in the first equality is the square root of the number of independent measurements.

Experimental setup.—The experimental setup, shown on the left in Fig. 1, has been assembled using two 1.3 GHz high-quality factor Q_0 SRF cavities. Both cavities are made out of bulk high residual resistivity ratio (RRR) > 200 niobium and have been prepared by bulk electropolishing, 800 °C annealing for 3 hours, light electropolishing, and a final 120 °C 48 hours baking. The cavities have been selected to have resonant frequencies of the fundamental TM_{010} modes as close to each other as possible. The mechanical holding structure has been designed in such a way as to minimize the frequency shifts of the receiver (bottom) cavity in response to liquid helium pressure fluctuations and mechanical vibrations, while allowing the emitter (top) cavity to be frequency tunable by tiny mechanical deformations. The cavities were oriented along a common axis and mounted 60 cm apart (center to center). An accelerator-style frequency tuner [17] assembly has been attached to the emitter cavity, allowing both "coarse" tuning by a stepper motor in a range of about 5 MHz with ~12 Hz resolution, as well as "fine-tuning" using the piezoelectric element in a range of about 8 kHz with ~0.1 Hz resolution [18]. Shielded microwave coaxial cables independently connect each cavity to room temperature signal generation and measurement electronics.

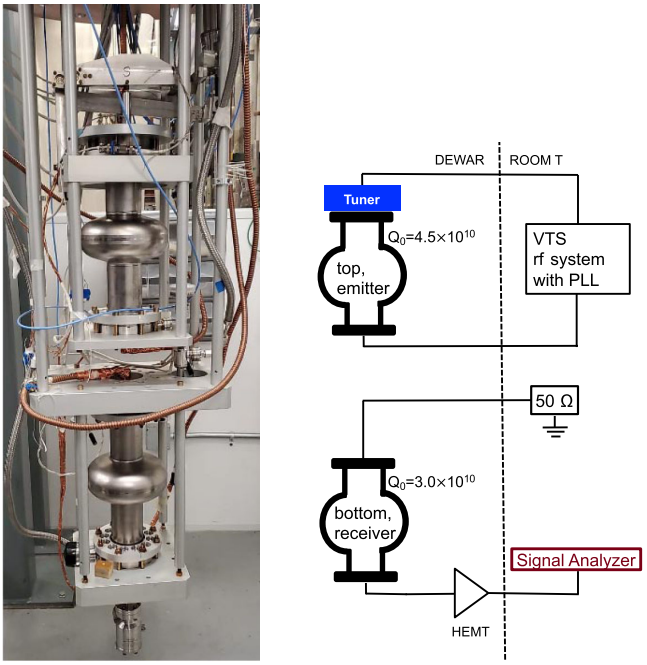

FIG. 1. Left: the experimental setup for the Dark SRF experiment consisting of two 1.3 GHz cavities. Right: a sketch of the Dark SRF electronic system.

Initially, both of the cavities were tested at 2 and 1.5 K in a liquid helium bath, using standard SRF techniques [19] to determine the fundamental mode frequencies and intrinsic quality factors Q_0, as well as the input (Q_{in}) and transmitted (Q_t) antennas external quality factors.

The emitter cavity rf ports were connected directly to incident and transmitted power cables of the rf system in Fermilab's Vertical Test Stand (VTS) and the corresponding phase lock loop (PLL) system. The incident and transmitted power cables were calibrated following the method explained in Ref. [19], Sec. II.A. In frequency stability runs, the receiver cavity input line included 30 dB attenuator to suppress room temperature thermal noise leaking into the cavity. The receiver cavity output rf port was connected to a high electron mobility transistor (HEMT) amplifier (LNF-LNC0.3_14A) with a nominal gain of 38 dB and noise temperature of 4 K at 5 K. From thermal noise measurements at 1.3 K (no rf power delivered to cavities) we estimated an effective gain of the HEMT, including attenuation of the connecting cables, to be 35 dB, corresponding to a total system noise temperature $T_{\mathrm{rec}} + T_{\mathrm{HEMT}} = 5.3$ K.

Frequency stability.—Frequency instability of the cavities may be separated into a slow drift on the timescale of minutes and more rapid variations known as microphonics. The frequency drift of the Dark SRF cavities was characterized by frequency stability runs during which the emitter cavity was driven on resonance with a PLL, and the

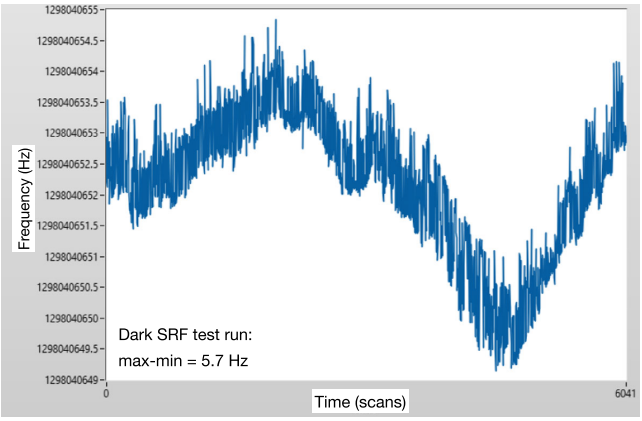

FIG. 2. The Dark SRF emitter frequency collected over 6041 scans (each lasting about a second). The frequency variation in this test spans 5.7 Hz. The emitter cavity was the less stable of the emitter-receiver pair.

resonant frequency was measured using a frequency counter. In a dozen such runs with $E_{\mathrm{acc}} = 6.4$ MV/m (corresponding to $U_{\mathrm{em}} = 0.6$ J), minimum-to-maximum emitter frequency variations between 3 and 8 Hz were observed at 2 K. No systematic difference was observed between the runs in which the frequencies were matched with the slow tuner and those with a piezoelectric actuator. A frequency stability test conducted within a day of the dark photon search showed frequency variations spanning 5.7 Hz over 100 min at 1.4 K, as shown in Fig. 2. Given the proximity of this measurement to the dark photon search, we take 5.7 Hz as a conservative input for the emitter drift in the analysis below. In addition, in a receiver frequency stability run only the receiver cavity was powered up and held at $E_{\mathrm{acc}} = 14$ kV/m for about 40 min. The resulting recorded minimum-to-maximum frequency variation was 3 Hz.

Microphonics measurements were presented in Ref. [18], with the cavity held on resonance by a PLL in VTS and its frequency being continuously measured. The observed rms frequency variations of 3 Hz and the characteristic jitter timescale of ~20–30 ms were observed. We take 3 Hz as the magnitude of microphonics in the analysis below, which—together with the slow drift—affects the experimental sensitivity, as discussed below.

Data taking.—Various system configurations were used to search for a dark photon. In each run, several steps were followed: (1) frequency matching, (2) dark photon search, (3) frequency recheck, (4) crosstalk check, and (5) thermal background measurement (if no crosstalk was seen). We discuss each step below.

For frequency matching, both cavities have been powered up by a single rf generator signal split into two routes. A phase lock loop has been used to have the rf generator follow the frequency of the emitter cavity, and the tuner mechanism has been applied to change the emitter cavity frequency until both emitter and receiver cavities are resonantly excited by the same signal, as observed with the signal analyzer connected to the receiver transmitted power line. Since the radiation pressure on the cavity walls changes the cavity frequency, as do small variations in the conditions in VTS, this procedure for frequency matching has been performed for each stored energy in the emitter cavity for the dark photon searches.

After frequency matching, the cable connecting the generator to the receiver cavity was disconnected, the receiver input line was terminated, and the measurement of the transmitted power from the receiver cavity was performed using a spectrum analyzer centered around the resonance frequency. The frequency sweeps in a window of 3 kHz with a resolution bandwidth of 1 Hz were utilized. Each scan used 10 000 points and took 1.83 s. Each data acquisition run lasted for ~30 min. This work presents the result of a $E_{\mathrm{acc}} = 6.2$ MV/m (corresponding to $U_{\mathrm{em}} = 0.6$ J of stored energy) run using the linear average of ~1300 frequency sweeps, in which no crosstalk noise was observed.

Upon conclusion of each dark photon search run, the physical cable connection between the generator and the receiver cavity input was reestablished to verify that the cavities remained frequency matched.

We have performed several additional measurements to evaluate the amount of crosstalk present in the system in each run. The phase lock was disengaged to allow the generator and the cavity to lose synchronization and the stored power in the emitted cavity to drop. If a peak of excess power seen in the receiver cavity moves to follow the frequency of the generator, the excess is deemed to be due to crosstalk. Crosstalk was suppressed after efforts to augment shielding in the signal lines, but it was still observed in some configurations. Shielding efforts continue; however, here, we focus on one configuration in which crosstalk was not observed. In the case when crosstalk was not observed, the power to the emitter was turned off to measure the thermal noise in the receiver cavity. Overall, several data acquisition runs were performed with the emitter field level in the range [20] $E_{\mathrm{acc}} = 6$–25 MV/m, equivalent to $U_{\mathrm{em}} = 0.6$–9.8 J of stored energy. We will present the results of one of the low power runs with $E_{\mathrm{acc}} = 6.2$ MV/m, $U_{\mathrm{em}} = 0.6$ J. Runs with higher stored fields exhibited a larger frequency drift and/or a significant amount of crosstalk.

Noise analysis.—Figure 3 shows spectra measured in both a thermal run (no excitation in the emitter cavity) and a search run. In both cases, a relatively flat power spectrum is observed with a peak centered at the frequency of the receiver cavity. This is the expected signal measured from a HEMT amplifier connected to a cavity that emits thermal photons around its resonant frequency. The peak was shown not to originate from crosstalk, and it also remained when the emitter power was turned off, signifying that it is background rather than signal.

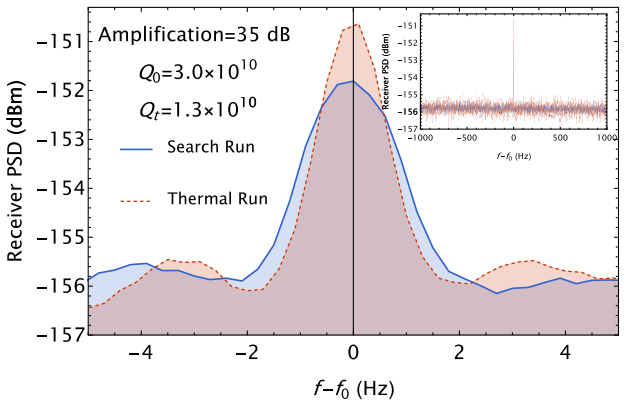

FIG. 3. The measured power spectral density (PSD) of the receiver cavity during the dark photon search run (blue) and thermal noise calibration run (red). For both runs, the peaks are caused by a leak of thermal photons from the receiver input line. The reference frequency is $f_0 = 1.298\,041$ GHz. The two peaks were shifted within the drifting modeling by 3.5 Hz to coincide. The signal region is ± 1.5 Hz around the peak. The power measured between the thermal run ($-151.6^{+0.23}_{-0.25}$ dBm) and search run ($-151.8^{+0.16}_{-0.17}$ dBm) is consistent with each other within 1σ.

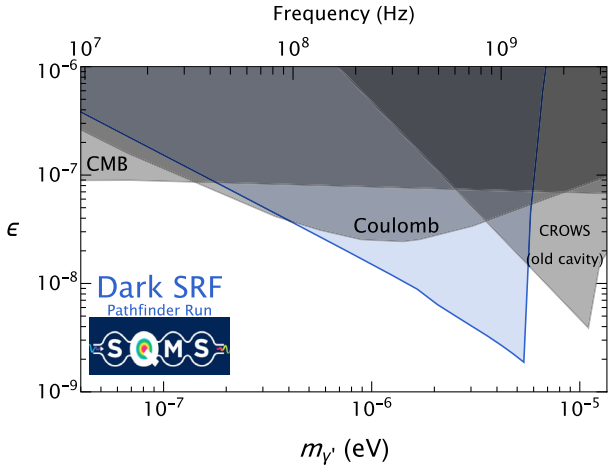

FIG. 4. The new 95% C.L. exclusion limit on dark photon parameter space. Our result is shown as the blue curve, where the region above is excluded. Also shown in gray are existing limits from the CROWS cavity experiment [8], measurements of the CMB [23–25], and tests of Coulomb's law [26,27].

In the $E_{\mathrm{acc}} = 6.2$ MV/m run, the emitter cavity was excited using a 1 W amplifier, achieving 0.6 J of stored energy. During the dark photon search, the receiver spectrum was well described by a flat background at -156 dBm of transmitted power P_t and a sharp peak of $P_t = -152$ dBm at the cavity frequency, as shown in Fig. 3. These values correspond to the power transmitted by the receiver cavity and include the 35 dB of amplification added by the HEMT on the P_t line. The flat background is consistent with the thermal noise in the HEMT amplifier, in both its power level and its variance (sampling over many frequencies).

The origin of the peak was identified to be a leak of thermal photons from the receiver input line (used to align the two cavities), which impacted our analysis in deriving the final result in the next section. This hypothesis was corroborated in a subsequent run in which the peak was removed by adding a 30 dB attenuator on the input line [21].

Results.—In the absence of a signal, this run was used to set a leading limit on the dark photon over a wide range of masses, as shown in Fig. 4. The limit setting procedure is described in the Appendix with the experimental parameter set shown in Table I. The receiver power, accounting for the power in the ± 1.5 Hz of the peak frequency after considering the amplification and quality factors in different subsystems, is $-187.0^{+0.16}_{-0.17}$ dBm, while from the thermal run we know the thermal power around the peak is $-186.8^{+0.23}_{-0.25}$ dBm. This allows us to put a limit on the signal power arising from a dark photon for a broad range of masses, predicted using Eq. (2). In particular, we demand that the signal power not exceed -186.7 dBm (not adding more than 0.3 dB beyond the measured -187.0 dBm during the dark photon search run) at 95% confidence level, using the modified frequentist confidence level (CLs) method [22] and Eq. (3).

The result is shown in Fig. 4. Our experiment excludes regions above the solid blue line. Compared to existing constraints from the cavity LSW experiment CROWS [8], measurements of the CMB [23–25] (note, however, that these bounds are slightly alleviated in various models of dark sectors [28]), and tests of Coulomb's law [26,27], our search provides the world's best limit and improves constraints on ϵ throughout the dark photon mass range of $m_{\gamma'} \simeq 2.1 \times 10^{-7}$–$5.7 \times 10^{-6}$ eV. We note that the improvement in ϵ sensitivity scales as $\mathrm{SNR}^{1/4}$, clearly showing that our setup is advantageous in many aspects. We stress, however, that this result is a first pathfinder experiment and there are several opportunities for improvement in forthcoming iterations, as discussed in the Conclusions.

We also note that this result, as well as any experiments sensitive to the longitudinal mode of the dark photon, can also be interpreted as a limit on the SM photon mass m_γ. This is because the dark photon longitudinal mode couples directly to SM charges, analogous to the longitudinal mode of a massive SM photon, but with a coupling suppressed by ϵ. In particular, for Dark SRF the formalism describing the production in the emitter cavity, screening in conducting shields, and signal generation in the receiver cavity is nearly identical between the two model scenarios if one equates $\epsilon m_{\gamma'} \simeq m_\gamma$ for $\epsilon \ll 1$. Thus, we find that the search described here provides a competitive direct laboratory limit on the SM photon mass [29], bounding it to be smaller than 8.6×10^{-15} eV $\simeq 1.5 \times 10^{-47}$ g. It has also been shown in Ref. [30] that this same setup can be sensitive

TABLE I. Table of key experimental parameters of the Dark SRF low power run used to set dark photon limits. Quality factors (intrinsic Q_0 and externals Q_{in}, Q_t) reported in the table are known within 10%. U for the emitter and receiver are the stored number of photons (equivalently, stored energy) in the equilibrium state of the cavities. P_{loss} is the power lost on the cavity walls, defined as $P_{\mathrm{injected}} - P_{\mathrm{transmitted}}$ or $P_{\mathrm{forward}} - P_{\mathrm{reflected}} - P_{\mathrm{transmitted}}$.

Parameter	Emitter	Receiver
Q_0	4.5×10^{10}	3.0×10^{10}
Q_{in}	1.8×10^{9}	4.5×10^{11}
Q_t	2.9×10^{11}	1.3×10^{10}
Frequency drift	5.7 Hz	3.0 Hz
Microphonics	3.1 Hz	3.1 Hz
P_{loss}	20 dBm	−187 dBm
U	6.7×10^{23}	5.3×10^{3}

to ultralight ($\ll 1$ meV) "millicharged" particles that are produced by the large electric fields of the emitter cavity. A simple estimate suggests that the run described here is sensitive to such particles with effective charges as small as $\sim$few $\times 10^{-9}$, roughly 2 orders of magnitude smaller than the best-existing laboratory bounds [31,32]. We will perform a dedicated analysis along these lines in future work.

Conclusions.—We present the first proof of concept experiment of a LSW experiment based on superconducting cavities. Our experiment was constructed based on high-quality factor SRF niobium cavities, and utilizing accelerator technology for high-precision frequency tuning allowed us to extend the exclusion boundary for the existence of dark photons in a broad range of rest masses and coupling constants.

Future improvements beyond this proof-of-concept run will be pursued. The utilization of ultrahigh-Q cavities introduces new and unique challenges in frequency stability and control. Bringing the frequency stability from a few hertz to the subhertz regime will significantly enhance the sensitivity. As frequency stability improves even further, beyond-state-of-the-art cavity coherence will lead to deeper sensitivity. In addition, further suppression of the crosstalk at higher emitter cavity powers can lead to higher signal powers. Placing the receiver cavity at millikelvin temperatures, inside a dilution refrigerator and coupled with a quantum-limited amplifier, will lead to lower noise level. Implementation of phase-sensitive readout can lead to an improved scaling of the SNR with integration time. The combination of these may lead to several more orders of magnitude of explored parameter space [33].

The authors would like to acknowledge help with measurements from Alexander Netepenko and help with numerical form factor calculations from Josh Isaacson and Will Jay. This material is based upon work supported by the U.S. Department of Energy, Office of Science, National Quantum Information Science Research Centers, Superconducting Quantum Materials and Systems Center (SQMS) under Contract No. DE-AC02-07CH11359.

Appendix: Signal strength calculation.—Here we present the calculation of the signal power in the receiver cavity using the formalism in Ref. [11]. For simplicity, we assume two identical cavities and focus on a particular cavity mode with frequency ω and with a field $\vec{E}(\vec{x},t) = \vec{E}_{\mathrm{cav}}(\vec{x})e^{i\omega t}$. The dark photon field sourced by the emitter cavity is approximately

$$\vec{E}'(\vec{r},t) \simeq -\epsilon m_{\gamma'}^2 \int_{V_{\mathrm{emitter}}} d^3x \frac{\vec{E}_{\mathrm{cav}}(\vec{x})}{4\pi|\vec{r}-\vec{x}|} e^{i(\omega t - k|\vec{r}-\vec{x}|)}, \quad \text{(A1)}$$

where V_{emitter} is the emitter cavity volume, and $k^2 = \omega^2 - m_{\gamma'}^2$. For $m_{\gamma'} > \omega$, $k = -i\sqrt{-\omega^2 + m_{\gamma'}^2}$.

The induced effective current density is

$$\vec{j}(\vec{r})e^{i\omega t} = -\frac{i\epsilon}{\omega}[m_{\gamma'}^2 \vec{E}' - \vec{\nabla}(\vec{\nabla}\cdot\vec{E}')]. \quad \text{(A2)}$$

In the limit where the emitter and receiver frequency match, the observable signal in the receiver cavity reads

$$\vec{E}_{\mathrm{receiver}}(\vec{r},t) = -\frac{Q_{\mathrm{rec}}}{\omega}\left[\frac{\int d^3x \vec{E}^*_{\mathrm{cav}}(\vec{x})\cdot\vec{j}(\vec{x})}{\int d^3x |\vec{E}_{\mathrm{cav}}(\vec{x})|^2}\right]\vec{E}_{\mathrm{cav}}(\vec{r})e^{i\omega t}, \quad \text{(A3)}$$

where the $\int d^3x$ integrates over the receiver cavity volume, and $\vec{E}_{\mathrm{cav}}(\vec{x})$ represents the electric field strength of a given receiver cavity mode. It is convenient to identify the (normalized) quantity in the square brackets above as a coupling or form factor:

$$|G|^2 \equiv \frac{1}{\epsilon^4}\left(\frac{\omega}{m_{\gamma'}}\right)^4 \left[\frac{\int d^3x \vec{E}^*_{\mathrm{cav}}(\vec{x})\cdot\vec{j}(\vec{x})}{\omega\int d^3x |\vec{E}_{\mathrm{cav}}(\vec{x})|^2}\right]^2, \quad \text{(A4)}$$

where the effective current $\vec{j}$ depends on receiver positioning $\vec{r}$, dark photon mass $m_{\gamma'}$, and ϵ. With our positioning and dark photon mass around ω, the longitudinal component dominates. The above considerations drive our parametrization of $|G|^2$, which makes $|G|^2$ independent of Q_{rec}, ϵ and $m_{\gamma'}$ to leading order.

In our experiments, we need to consider the frequency spread from both the emitter and the receiver, the frequency drift over time, and frequency jittering due to other mechanical effects such as bubble collisions. These effects can be *conservatively* [34] modeled as a mismatch between receiver frequency and emitter frequency, effectively reducing the form factor $|G|^2$ by

$$|G|^2 \to \frac{\omega^2}{\omega^2 + 4\delta_\omega^2 Q_{\rm rec}^2}|G|^2, \tag{A5}$$

where δ_ω represents a typical mismatch in (angular) frequency. For our run that determines the new results, the frequency mismatch is conservatively assumed to be 7.8 Hz (from frequency drift and jittering). With the resonant frequency of 1.3 GHz, and receiver cavity intrinsic Q factor of 3×10^{10}, jittering causes a suppression of the signal power by a factor of 7.7×10^{-6}.

*aroman@fnal.gov
†roni@fnal.gov
‡annag@fnal.gov
§zliuphys@umn.edu

[1] B. Holdom, Phys. Lett. B **166**, 196 (1986).
[2] J. Jaeckel and A. Ringwald, Annu. Rev. Nucl. Part. Sci. **60**, 405 (2010).
[3] A. Caputo, A. J. Millar, C. A. J. O'Hare, and E. Vitagliano, Phys. Rev. D **104**, 095029 (2021).
[4] L. B. Okun, Sov. Phys. JETP **56**, 502 (1982).
[5] K. Van Bibber, N. R. Dagdeviren, S. E. Koonin, A. K. Kerman, and H. N. Nelson, Phys. Rev. Lett. **59**, 759 (1987).
[6] F. Hoogeveen and T. Ziegenhagen, Nucl. Phys. **B358**, 3 (1991).
[7] K. Ehret *et al.* (ALPS Collaboration), Nucl. Instrum. Methods Phys. Res., Sect. A **612**, 83 (2009).
[8] M. Betz, F. Caspers, M. Gasior, M. Thumm, and S. W. Rieger, Phys. Rev. D **88**, 075014 (2013).
[9] S. R. Parker, J. G. Hartnett, R. G. Povey, and M. E. Tobar, Phys. Rev. D **88**, 112004 (2013).
[10] J. Jaeckel and A. Ringwald, Phys. Lett. B **659**, 509 (2008).
[11] P. W. Graham, J. Mardon, S. Rajendran, and Y. Zhao, Phys. Rev. D **90**, 075017 (2014).
[12] H. S. Padamsee, Annu. Rev. Nucl. Part. Sci. **64**, 175 (2014).
[13] A. Romanenko, A. Grassellino, A. C. Crawford, D. A. Sergatskov, and O. Melnychuk, Appl. Phys. Lett. **105**, 234103 (2014).
[14] A. Romanenko, R. Pilipenko, S. Zorzetti, D. Frolov, M. Awida, S. Belomestnykh, S. Posen, and A. Grassellino, Phys. Rev. Appl. **13**, 034032 (2020).
[15] As was also pointed out in Ref. [11], the axion search conducted by CROWS was arranged longitudinally and may be reinterpreted to give a stronger dark photon limit at low masses.
[16] R. H. Dicke, Rev. Sci. Instrum. **17**, 268 (1946).
[17] Y. Pischalnikov, E. Borissov, I. Gonin, J. Holzbauer, T. Khabiboulline, W. Schappert, S. Smith, and J. Yun, in *Proceedings of the 6th International Particle Accelerator Conference, WEPTY035* (JACoW, Richmond, 2015).
[18] Y. Pischalnikov, D. Bice, A. Grassellino, T. Khabiboulline, O. Melnychuk, R. Pilipenko, S. Posen, O. Pronichev, and A. Romanenko, in *Proceedings of the 19th International Conference on RF Superconductivity, TUP085* (JACoW, Dresden, 2019).
[19] O. Melnychuk, A. Grassellino, and A. Romanenko, Rev. Sci. Instrum. **85**, 124705 (2014).
[20] We use $E_{\rm acc}$, the effective electric field seen by a charged particle traversing the cavity on its central axis, to facilitate the comparison with state-of-the-art SRF accelerator cavities. For the mode in question, this field is related to the peak field by $E_{\rm peak} \simeq 1.8 E_{\rm acc}$.
[21] The runs with this lower thermal background encountered a larger crosstalk peak and were thus not used to set the strongest limit.
[22] R. L. Workman *et al.* (Particle Data Group), Prog. Theor. Exp. Phys. **2022**, 083C01 (2022).
[23] A. Mirizzi, J. Redondo, and G. Sigl, J. Cosmol. Astropart. Phys. 03 (2009) 026.
[24] A. Caputo, H. Liu, S. Mishra-Sharma, and J. T. Ruderman, Phys. Rev. Lett. **125**, 221303 (2020).
[25] A. A. Garcia, K. Bondarenko, S. Ploeckinger, J. Pradler, and A. Sokolenko, J. Cosmol. Astropart. Phys. 10 (2020) 011.
[26] E. R. Williams, J. E. Faller, and H. A. Hill, Phys. Rev. Lett. **26**, 721 (1971).
[27] S. A. Abel, M. D. Goodsell, J. Jaeckel, V. V. Khoze, and A. Ringwald, J. High Energy Phys. 07 (2008) 124.
[28] A. Berlin, J. A. Dror, X. Gan, and J. T. Ruderman, J. High Energy Phys. 05 (2023) 046.
[29] R. L. Workman *et al.* (Particle Data Group), Prog. Theor. Exp. Phys. **2022**, 083C01 (2022).
[30] A. Berlin and A. Hook, Phys. Rev. D **102**, 035010 (2020).
[31] M. Ahlers, H. Gies, J. Jaeckel, and A. Ringwald, Phys. Rev. D **75**, 035011 (2007).
[32] F. Della Valle, E. Milotti, A. Ejlli, G. Messineo, L. Piemontese, G. Zavattini, U. Gastaldi, R. Pengo, and G. Ruoso, Phys. Rev. D **90**, 092003 (2014).
[33] A. Berlin *et al.*, arXiv:2203.12714.
[34] Jittering, for instance, can be modeled as a reduction of integration time, which would be a lesser suppression than what we use here.